AMERICAN SOCIETY FOR MICROBIOLOGY | Journal of Virology®

PATHOGENESIS AND IMMUNITY

Simian Immunodeficiency Virus Persistence in Cellular and Anatomic Reservoirs in Antiretroviral Therapy-Suppressed Infant Rhesus Macaques

Maud Mavigner,[a] Jakob Habib,[a] Claire Deleage,[b] Elias Rosen,[c] Cameron Mattingly,[a] Katherine Bricker,[a] Angela Kashuba,[c] Franck Amblard,[a] Raymond F. Schinazi,[a] Benton Lawson,[d] Thomas H. Vanderford,[d] Sherrie Jean,[d] Joyce Cohen,[d] Colleen McGary,[d] Mirko Paiardini,[d] Matthew P. Wood,[e] Donald L. Sodora,[e] Guido Silvestri,[d] Jacob Estes,[b,f] Ann Chahroudi[a,d,g]

[a]Department of Pediatrics and Center for AIDS Research, Emory University School of Medicine, Atlanta, Georgia, USA

[b]AIDS and Cancer Virus Program, Frederick National Laboratory for Cancer Research, Leidos Biomedical Research, Inc., Frederick, Maryland, USA

[c]Eshelman School of Pharmacy, University of North Carolina, Chapel Hill, North Carolina, USA

[d]Yerkes National Primate Research Center, Emory University, Atlanta, Georgia, USA

[e]Center for Infectious Disease Research, Seattle, Washington, USA

[f]Vaccine and Gene Therapy Institute and Oregon National Primate Research Center, Oregon Health and Science University, Beaverton, Oregon, USA

[g]Emory+Children's Center for Childhood Infections and Vaccines, Atlanta, Georgia, USA

ABSTRACT Worldwide, nearly two million children are infected with human immunodeficiency virus (HIV), with breastfeeding accounting for the majority of contemporary HIV transmissions. Antiretroviral therapy (ART) has reduced HIV-related morbidity and mortality but is not curative. The main barrier to a cure is persistence of latent HIV in long-lived reservoirs. However, our understanding of the cellular and anatomic sources of the HIV reservoir during infancy and childhood is limited. Here, we developed a pediatric model of ART suppression in orally simian immunodeficiency virus (SIV)-infected rhesus macaque (RM) infants, with measurement of virus persistence in blood and tissues after 6 to 9 months of ART. Cross-sectional analyses were conducted to compare SIV RNA and DNA levels in adult and infant RMs naive to treatment and on ART. We demonstrate efficient viral suppression following ART initiation in SIV-infected RM infants with sustained undetectable plasma viral loads in the setting of heterogeneous penetration of ART into lymphoid and gastrointestinal tissues and low drug levels in the brain. We further show reduction in SIV RNA and DNA on ART in lymphoid tissues of both infant and adult RMs but stable (albeit low) levels of SIV RNA and DNA in the brains of viremic and ART-suppressed infants. Finally, we report a large contribution of naive $CD4^+$ T cells to the total CD4 reservoir of SIV in blood and lymph nodes of ART-suppressed RM infants that differs from what we show in adults. These results reveal important aspects of HIV/SIV persistence in infants and provide insight into strategic targets for cure interventions in a pediatric population.

IMPORTANCE While antiretroviral therapy (ART) can reduce HIV replication, the virus cannot be eradicated from an infected individual, and our incomplete understanding of HIV persistence in reservoirs greatly complicates the generation of a cure for HIV infection. Given the immaturity of the infant immune system, it is critically important to study HIV reservoirs specifically in this population. Here, we established a pediatric animal model to simulate breastfeeding transmission and study SIV reservoirs in rhesus macaque (RM) infants. Our study demonstrates that ART can be safely administered to infant RMs for prolonged periods and that it efficiently controls viral replication in this model. SIV persistence was shown in blood and tissues, with similar

Received 4 April 2018 **Accepted** 29 June 2018

Accepted manuscript posted online 11 July 2018

Citation Mavigner M, Habib J, Deleage C, Rosen E, Mattingly C, Bricker K, Kashuba A, Amblard F, Schinazi RF, Lawson B, Vanderford TH, Jean S, Cohen J, McGary C, Paiardini M, Wood MP, Sodora DL, Silvestri G, Estes J, Chahroudi A. 2018. Simian immunodeficiency virus persistence in cellular and anatomic reservoirs in antiretroviral therapy-suppressed infant rhesus macaques. J Virol 92:e00562-18. https://doi.org/10.1128/JVI.00562-18.

Editor Viviana Simon, Icahn School of Medicine at Mount Sinai

Address correspondence to Ann Chahroudi, achahro@emory.edu.

[This article was published on 29 August 2018 with a byline that lacked Benton Lawson and Thomas H. Vanderford. The byline was updated in the current version, posted on 14 November 2018.]

anatomic distributions of SIV reservoirs in infant and adult RMs. However, in the peripheral blood and lymph nodes, a greater contribution of the naive CD4$^+$ T cells to the SIV reservoir was observed in infants than in adults.

KEYWORDS antiretroviral therapy, SIV, infants, rhesus macaques

In 2016, 2.1 million children were living with human immunodeficiency virus (HIV) infection and 160,000 children were newly infected by the virus. In the absence of treatment, a more rapid tempo of disease is observed in pediatric HIV infection than in adults, with higher peak and set point viral loads during the first years of life, leading to death in 50% of untreated HIV-infected children by the age of 2 years (1–4). Several factors might account for this rapid disease progression, including high rates of virus production and CD4$^+$ T cell turnover, as well as weaker HIV-specific immune responses. As in HIV-infected adults, antiretroviral therapy (ART) has greatly reduced HIV-related morbidity and mortality in children, but it is not curative due to the persistence of latent virus in cellular and anatomic reservoirs. Children face the prospect of lifelong ART with the associated difficulties of limited pediatric drug formulations, drug adherence requirements during challenging developmental stages, and potential adverse medication effects. As such, HIV cure/remission represent especially important goals for the pediatric population.

In 2014, absence of detectable viremia following ART cessation was reported in a perinatally HIV-infected child treated for 18 months starting 30 h after birth (5, 6). Although the virus levels ultimately rebounded 28 months after ART interruption, this case raised hope for the potential of remission in perinatal HIV infection that is treated early. There have since been several other notable pediatric case reports of potential HIV remission (7–10), but clear evidence for a generalizable approach to eliminate HIV reservoirs in infants and children is lacking. Particularly with late gestation and intrapartum HIV transmission, the capacity to treat soon after infection makes the pediatric setting favorable for cure approaches that incorporate early ART. However, due to increased efforts to prevent mother-to-child transmission of HIV and interventions used during pregnancy and delivery, the rates of *in utero* and intrapartum transmission have decreased in recent years. As a result, over 50% of new pediatric HIV infections occur through breastfeeding (11). As infants infected via breastfeeding are frequently diagnosed late and ART initiation is delayed, studies of reservoirs and cure interventions in this setting are greatly needed.

The specificities of the developing immune system provide a unique setting for HIV cure research. The dynamics of HIV persistence in children may differ from those in adults, due to different types and numbers of target cells, a bias toward immune tolerance, lower immune activation than in adults, a reduced T cell memory compartment, and distinct pharmacokinetics of ART in blood and tissues. In adults, the best-characterized HIV reservoir consists of a small pool of latently infected memory CD4$^+$ T cells carrying transcriptionally silent but replication-competent HIV (12–15). The HIV reservoir has been extensively studied in HIV-infected adults, as it represents the main barrier to a cure. However, little is known about the cellular and anatomic distribution of the HIV reservoir in the pediatric population. Given the difficulties in studying young children, development of specific pediatric animal models is critical.

Models of simian immunodeficiency virus (SIV) infection of adult macaques are well established and robust and possess many similarities to HIV infection in terms of transmission, acute/early infection events, viral and CD4$^+$ T cell dynamics, and disease progression. Using an optimized ART regimen, several groups have demonstrated consistent suppression of plasma viral loads in rhesus macaques (RMs) with viral dynamics that replicate those of ART-treated, HIV-infected patients (16–19), thus allowing the RMs to be used as a translational animal model for HIV cure studies. In the present study, we developed a pediatric model of oral transmission of SIV followed by ART suppression of viremia. Using this model and in comparison to cohorts of viremic RM infants, as well as viremic and ART-suppressed adult RMs, we show (i) safety and

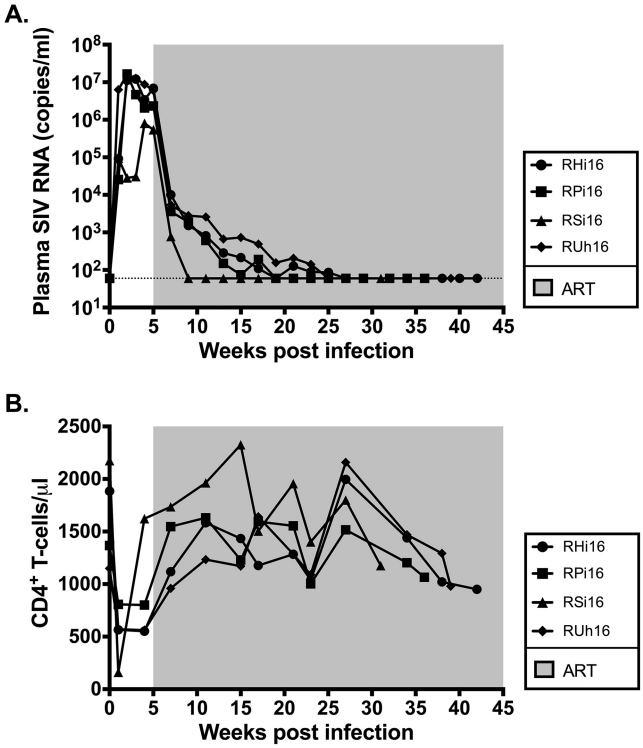

FIG 1 SIV-infected infant RM virologic and immunologic response to ART. (A) Longitudinal analysis of plasma SIV RNA levels. The shaded area represents the period of ART treatment. The dotted line represents the limit of detection of the assay. (B) Longitudinal analysis of peripheral $CD4^+$ T cell absolute counts. The shaded area represents the period of ART treatment.

efficacy of ART in SIV-infected infant RMs; (ii) variable penetration of ART in tissues, with very low drug levels found in brain; (iii) an expected reduction in SIV RNA and DNA on ART in lymphoid tissues, but no change in viral levels in the brains of RM infants; and (iv) an enhanced contribution of naive $CD4^+$ T cells to the total CD4 reservoir of SIV in infants compared to adults. These results inform our understanding of HIV/SIV persistence in infants and suggest that remission-directed strategies for this age group may need to consider naive T cells.

RESULTS

Experimental design. To establish an infant model of breastfeeding transmission and ART suppression of viremia, four infant Indian RMs (three males and one female) were exposed to two consecutive doses of 10^5 50% tissue culture infective doses ($TCID_{50}$) SIV_{mac251} by orogastric administration at 20 to 21 weeks of age. Starting at day 35 postinfection, all four RMs were initiated on ART. ART was started during early chronic infection to simulate a "real-world" timeline of breastfeeding transmission and diagnosis and to allow maximal establishment of SIV reservoirs (20–22). The ART regimen consisted of two reverse transcriptase inhibitors (tenofovir [PMPA] at 20 mg/kg of body weight/day and emtricitabine [FTC] at 40 mg/kg/day) and one integrase inhibitor (dolutegravir [DTG] at 2.5 mg/kg/day) coformulated into a single dose administered once daily by subcutaneous injection. The drug doses were based on prior experience and published literature for adult macaques, and it should be noted that, of the three drugs used, only FTC has FDA-approved dosing guidelines for the age group studied here (https://aidsinfo.nih.gov/guidelines/html/2/pediatric-arv/0). The RMs were euthanized on ART 6 to 9 months postinfection, and detailed necropsy was performed to thoroughly quantify SIV reservoirs and measure drug penetration in various tissues.

Efficiency and safety of the ART regimen in SIV-infected infant RMs. As shown in Fig. 1A, following experimental infection with SIV_{mac251}, the four infant RMs expe-

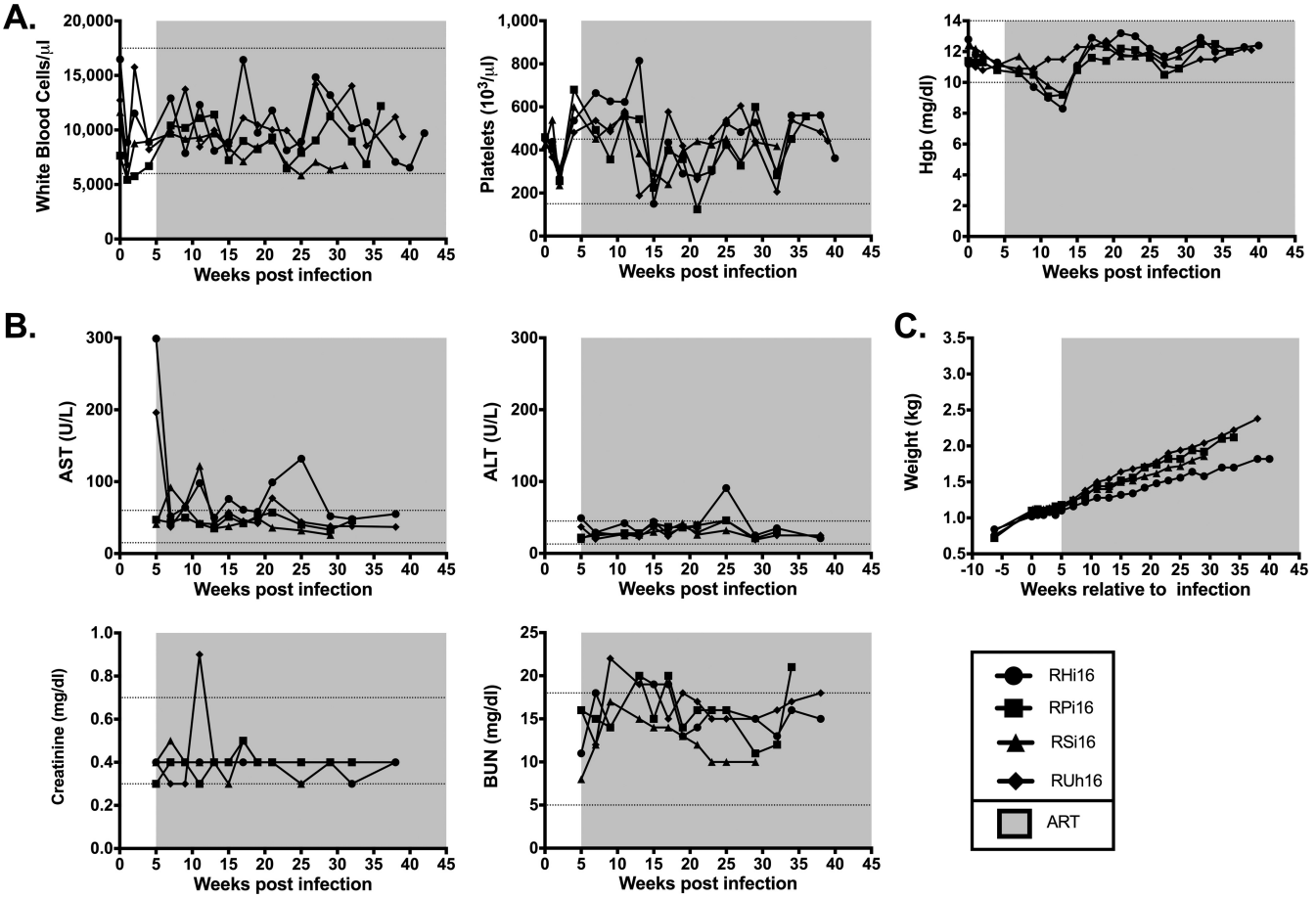

FIG 2 Safety data in ART-treated SIV-infected RM infants. Longitudinal assessment of complete blood counts (Hgb, hemoglobin levels) (A), serum chemistries (B), and body weight (C). The shaded areas represent the period of ART treatment. The dotted lines represent the normal range for each parameter.

rienced a rapid, exponential increase in virus replication that peaked at weeks 2 to 4 postinfection (10^6 to 10^7 SIV RNA copies/ml plasma). Following ART initiation at week 5 after infection, we observed a 2 to 3 log reduction in plasma viral loads within 2 weeks and levels below the limit of detection of our assay (60 copies/ml plasma) after 4 to 22 weeks of treatment. Consistent with prior studies of SIV infection in adult RMs (17, 23), the absolute number of peripheral $CD4^+$ T cells was significantly decreased following infection (1,644 ± 203 preinfection versus 916 ± 101 pre-ART; $P = 0.006$) (Fig. 1B) and was partially restored on ART (916 ± 101 pre-ART versus 1,441 ± 81 on ART; $P = 0.0003$) (Fig. 1B). The four RM infants demonstrated normal levels of white blood cells throughout the treatment period (Fig. 2A). Platelet counts, while high at ART initiation, tended to normalize during treatment (Fig. 2A), and no clinical thrombotic events occurred. Three of four RM infants became anemic following the period of intensive blood sampling, but hemoglobin returned to normal levels for the remainder of the study (Fig. 2A). Hepatic and renal functions were not adversely impacted by ART, as indicated by serum levels of aspartate transaminase (AST), alanine transaminase (ALT), creatinine, and blood urea nitrogen (BUN) (Fig. 2B), with only transient elevations in these parameters in 1 or 2 animals. Finally, SIV-infected RM infants demonstrated steady weight gain after ART initiation (Fig. 2C), with weights within the low-normal range or slightly below normal at selected time points (which is not unexpected during SIV infection). Altogether, these results show that ART was well tolerated by infant RMs and was efficient at reducing SIV replication within a time frame similar to that for HIV-infected infants (24, 25), resulting in partial reconstitution of the peripheral $CD4^+$ T cell pool.

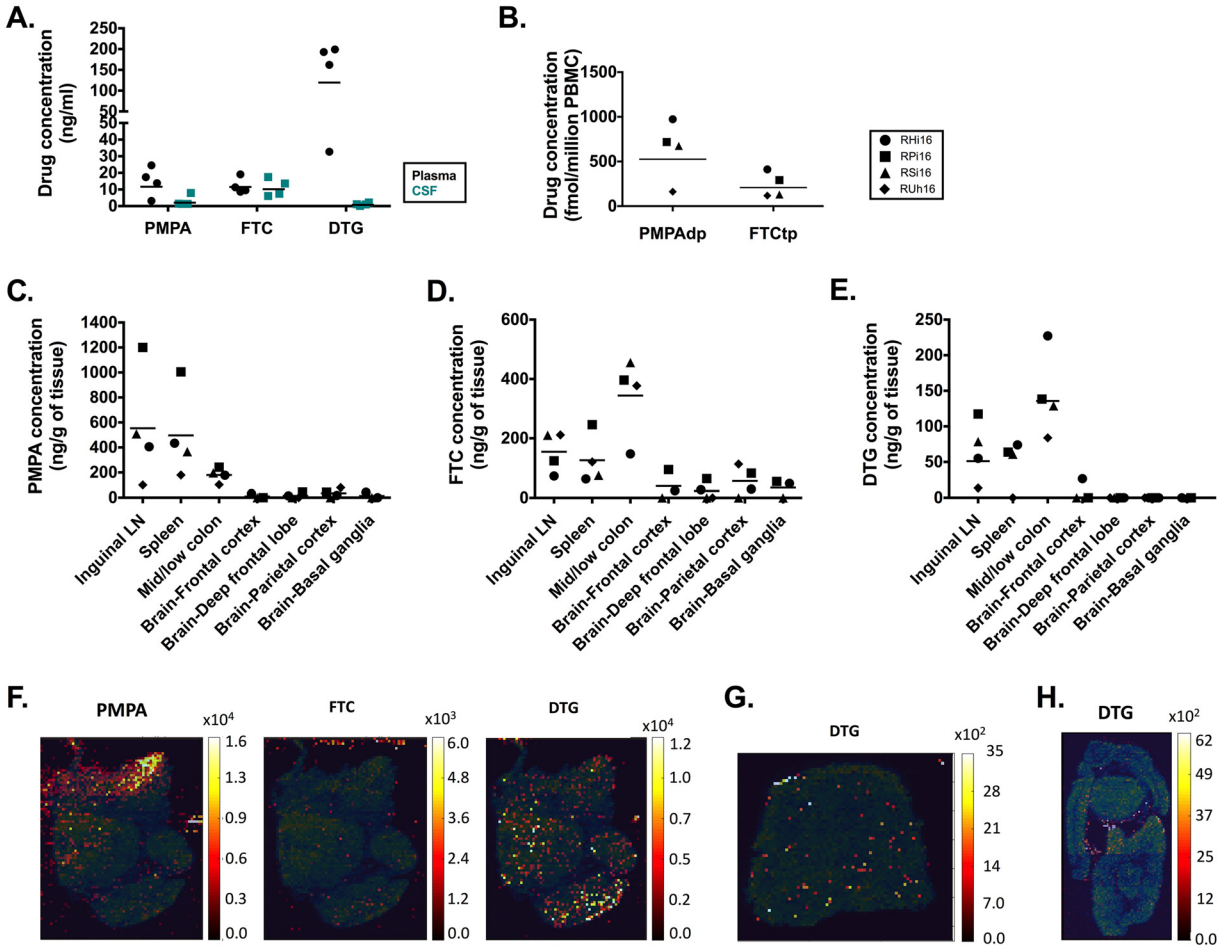

FIG 3 Antiretroviral drug levels in fluids and tissues of ART-treated SIV-infected RM infants. (A) Levels of PMPA, FTC, and DTG in the plasma and CSF. (B) Levels of phosphorylated metabolites of FTC and PMPA (FTCtp and PMPAdp) in PBMCs. (C, D, and E) Levels of PMPA (C), FTC (D), and DTG (E) in tissue measured by LS-MS/MS in the LN, spleen, colon, and brain. The horizontal lines represent medians. (F, G, and H) Representative IR-MALDESI images of ART distribution in lymph nodes (F), spleen (G), and colon (H). The distribution of the drugs is depicted using a color scale ranging from dark red for areas of low concentration to yellow for areas of high concentration. The maps are overlaid on the ion map for cholesterol (blue-green color scale).

Drug concentrations in blood and tissues of ART-treated SIV-infected RM infants. We next measured antiretroviral drug levels in fluids and tissues using both liquid chromatography-tandem mass spectrometry (LS-MS/MS) and infrared matrix-assisted laser desorption-electrospray ionization (IR-MALDESI) techniques (26). Trough plasma concentrations of PMPA, FTC, and DTG measured by LS-MS/MS are shown in Fig. 3A. These measured values are below published ranges for the same drugs dosed orally in children (27–29); however, it is important to recall that plasma viral loads were below the limit of detection at the time of this analysis, meaning that the combination ART regimen was effective in suppressing viremia in infant RMs. In the cerebrospinal fluid (CSF), trough levels of PMPA and DTG were lower than in plasma, with levels of DTG near or below the limit of quantification of the LS-MS/MS method in three of four animals (Fig. 3A); however, CSF viral loads were undetectable in all the animals at the same time point (data not shown). Since PMPA and FTC are rapidly converted to active drug metabolites inside the cell, we also measured PMPA-diphosphate (PMPAdp) and FTC-5′-triphosphate (FTCtp) in peripheral blood mononuclear cells (PBMCs) of the four infant RMs (Fig. 3B). FTCtp levels were similar to or lower than those found in healthy adults (30, 31), but reference data for children are not available. The observed levels of PMPAdp in three animals were much higher than has been reported for HIV-infected children (28), possibly reflecting a higher dose used in the macaques than is recommended for pediatric clinical practice.

We then assessed drug penetration in lymph nodes (LN), spleen, colon, and brain using LS-MS/MS and IR-MALDESI, a technique that allows the spatial visualization of the anatomic distribution of the drugs within the tissue (26). LS-MS/MS analyses showed detectable levels of all three drugs in the lymphoid tissues and colon but very low to undetectable levels in the brain (Fig. 3C to E). Higher, but variable, levels of PMPA were found in LN and spleen than in the colon (Fig. 3C). Conversely, FTC and DTG distribution was slightly greater in the colon than in the lymphoid tissues (Fig. 3D and E). The animal (RUh16) with the lowest plasma trough level of DTG also had the lowest levels of DTG measured in LN, spleen, and colon.

In the LN, IR-MALDESI analyses depicted a heterogeneous distribution of both DTG and PMPA, with PMPA concentrated in the medullary sinuses (Fig. 3F). In the spleen, IR-MALDESI confirmed diffuse low levels of DTG (Fig. 3G), but PMPA and FTC could not be visualized by this method (data not shown). DTG appeared to concentrate along the mucosa of the colon by IR-MALDESI (Fig. 3H), with PMPA and FTC again below the limit of quantification. None of the drugs could be detected by IR-MALDESI across all the brain sections assessed (deep frontal lobe, frontal cortex, parietal cortex, and basal ganglia) in the infants (data not shown). An important caveat to this work is that, due to rapid degradation of the phosphorylated active metabolites of PMPA and FTC, all IR-MALDESI measurements were of the parent drug.

SIV RNA and DNA persistence in tissues. To better define the tissue compartments contributing to SIV persistence in ART-treated RM infants, we performed RNAscope and DNAscope *in situ* hybridization to quantify SIV RNA$^+$ and DNA$^+$ cells, respectively, in various lymphoid and nonlymphoid tissues (32). We used this highly sensitive and specific approach to compare the levels of SIV DNA and RNA in the LN, spleen, brain, and gut compartments of the four ART-suppressed SIV-infected RM infants (cohort A) to those in independent cohorts of viremic ART-naive SIV-infected RM infants (cohort B), ART-suppressed SIV-infected RM adults (cohort C), and viremic ART-naive SIV-infected RM adults (cohort D) (Table 1).

Viral DNA$^+$ (vDNA$^+$) cells were found for all the animals tested in all tissues with no restriction in the anatomic location (Fig. 4A). Comparing vDNA levels in primary lymphoid tissues (LN B-cell follicle, LN T cell zone, spleen follicle, and gut lymphoid aggregates), the numbers of vDNA$^+$ cells in ART-suppressed infant RMs were similar to those found in ART-suppressed adults but were significantly lower than those observed in both viremic infants ($P = 0.0024$) and viremic adults ($P < 0.0001$) (Fig. 4B). In contrast, similar levels of vDNA$^+$ cells were found in the gut lamina propria and in the brain in the ART-suppressed and viremic infant RMs (Fig. 4B), as well as ART-suppressed and viremic adult RMs (Fig. 4B).

In ART-suppressed RM infants, low levels of SIV RNA were detected in all the tissues analyzed (Fig. 5A). The cross-sectional comparison showed no statistical difference in the numbers of vRNA$^+$ cells in any tissue between ART-suppressed infants and ART-suppressed adults. Reduced levels of SIV RNA$^+$ cells were observed in ART-suppressed infant RMs compared to viremic infant RMs in the primary lymphoid tissues ($P < 0.0001$) and spleen red pulp ($P = 0.0111$) (Fig. 5B). Interestingly, while already at low levels in viremic animals, the number of vRNA$^+$ cells did not decline in the brains of ART-suppressed infant RMs compared to viremic infant RMs (Fig. 5B), whereas a reduction was observed in ART-suppressed adults compared to viremic adults ($P = 0.0318$). The lack of reduction of SIV RNA$^+$ and DNA$^+$ cell levels in the brains of ART-suppressed compared to viremic RM infants is consistent with low to undetectable drug levels seen in the brain.

We then assessed the phenotype of the cells harboring vRNA for all ART-suppressed infants in the LN and brain tissues. Unsurprisingly, only CD4$^+$ T cells were found to harbor vRNA in the LN (Fig. 6A). Only microglial cells, identified using Iba1 antibody (Ab), were found to be vRNA$^+$ within all brain compartments (frontal lobe, deep frontal lobe, parietal cortex, and basal ganglia) (Fig. 6B). Since the RNAscope approach allowed us to visualize individual virions, we quantified the single particles trapped within the

TABLE 1 Animal characteristics

Cohort	ID	Sex[a]	Age at infection	Virus	Route of infection	Infectious dose	ART			Time postinfection (wk)	Viral load (copies/ml)	CD4 count (cells/mm^3)
							Regimen[b]	Initiation (days p.i.)	Duration (wk)			
A (ART-suppressed infants)	RHi16	M	4.7 mo	SIV_{mac251}	Oral	1E5 $TCID_{50}$	PMPA/FTC/DTG	35	37	42	<60	950
	RPi16	F	4.6 mo	SIV_{mac251}	Oral	1E5 $TCID_{50}$	PMPA/FTC/DTG	35	31	36	<60	1,065
	RSi16	M	4.6 mo	SIV_{mac251}	Oral	1E5 $TCID_{50}$	PMPA/FTC/DTG	35	26	31	<60	1,176
	RUh16	M	5 mo	SIV_{mac251}	Oral	1E5 $TCID_{50}$	PMPA/FTC/DTG	35	33	38	<60	979
	Median		4.7 mo					35	32	37		1,022
B (viremic infants)	A14203	M	2.5 mo	SIV_{mac251}	Oral	4E3 $TCID_{50}$	NA	NA	NA	15	2.20E+07	3,778
	A14115	M	4.0 mo	SIV_{mac251}	Oral	1E4 $TCID_{50}$	NA	NA	NA	17	9.18E+06	3,300
	A14112	M	4.0 mo	SIV_{mac251}	Oral	1E4 $TCID_{50}$	NA	NA	NA	18	3.70E+05	1,296
	A14113	F	4.0 mo	SIV_{mac252}	Oral	1E4 $TCID_{50}$	NA	NA	NA	18	6.17E+07	3,400
	Median		3.6 mo							17		3,350
C (ART-suppressed adults)	RYb13	F	4.35 yr	SIV_{mac251}	i.v.	1E3 $TCID_{50}$	PMPA/FTC/RAL/MVC/DRV/r	52	60	68	<60	635
	RAi13	F	4.33 yr	SIV_{mac251}	i.v.	1E3 $TCID_{50}$	PMPA/FTC/RAL/MVC/DRV/r	51	61	68	166	374
	RPa10	F	10.44 yr	SIV_{mac251}	i.v.	1E3 $TCID_{50}$	PMPA/FTC/RAL/DRV/r	45	35	55	<60	463
	RZm11	F	7.34 yr	SIV_{mac251}	i.v.	1E3 $TCID_{50}$	PMPA/FTC/RAL/MVC/DRV/r	51	58	65	<60	194
	RPa13	F	4.44 yr	SIV_{mac251}	i.v.	1E3 $TCID_{50}$	PMPA/FTC/RAL/MVC/DRV/r	51	47	55	<60	728
	RJf13	F	4.35 yr	SIV_{mac251}	i.v.	1E3 $TCID_{50}$	PMPA/FTC/RAL/MVC/DRV/r	51	47	54	<60	490
	RWo10	F	9.50 yr	SIV_{mac251}	i.v.	1E3 $TCID_{50}$	PMPA/FTC/RAL/DRV/r	45	34	34	<60	614
	RSz12	F	5.30 yr	SIV_{mac251}	i.v.	1E3 $TCID_{50}$	PMPA/FTC/RAL/MVC/DRV/r	52	31	39	<60	359
	Median		6.3 yr					50	47	51		477
D (viremic adults)	RPz10	M	4.3 yr	SIV_{mac239}	i.r.	1E4 $TCID_{50}$	NA	NA	NA	55	1.44E+05	99
	DEJW	M	3.6 yr	SIV_{mac239}	i.v.	2.2E5 IU	NA	NA	NA	89	5.00E+09	214
	RPt10	M	5.1 yr	SIV_{mac239}	i.r.	1E4 $TCID_{50}$	NA	NA	NA	52	1.43E+04	391
	RGd11	M	4 yr	SIV_{mac239}	i.r.	1E4 $TCID_{50}$	NA	NA	NA	65	2.34E+05	948
	H090	M	3.4 yr	SIV_{mac239}	i.v.	2.2E5 IU	NA	NA	NA	89	6.00E+09	230
	RAy10	M	4.6 yr	SIV_{mac239}	i.r.	1E4 $TCID_{50}$	NA	NA	NA	57	1.58E+06	613
	RYn10	F	4.8 yr	SIV_{mac239}	i.r.	1E4 $TCID_{50}$	NA	NA	NA	51	6.38E+06	132
	Median		4.3 yr							65	1.58E+06	230
E (ART-suppressed adults)	150-12R	M	3 yr	SIV_{mac251}	i.v.	1E3 $TCID_{50}$	PMPA/FTC/DTG	11	24	25	<60	588
	182-12R	F	3.1 yr	SIV_{mac251}	i.v.	1E3 $TCID_{50}$	PMPA/FTC/DTG	11	25	26	<60	572
	192-12R	F	3.1 yr	SIV_{mac251}	i.v.	1E3 $TCID_{50}$	PMPA/FTC/DTG	11	24	26	<60	469
	208-12R	M	3.1 yr	SIV_{mac251}	i.v.	1E3 $TCID_{50}$	PMPA/FTC/DTG	11	25	27	<60	357
	Median		3.1 yr					11	25	26		521

[a]M, male; F, female.
[b]PMPA, tenofovir; FTC, emtricitabine; RAL, raltegravir; DRV/r, darunavir/ritonavir; MVC, maraviroc.

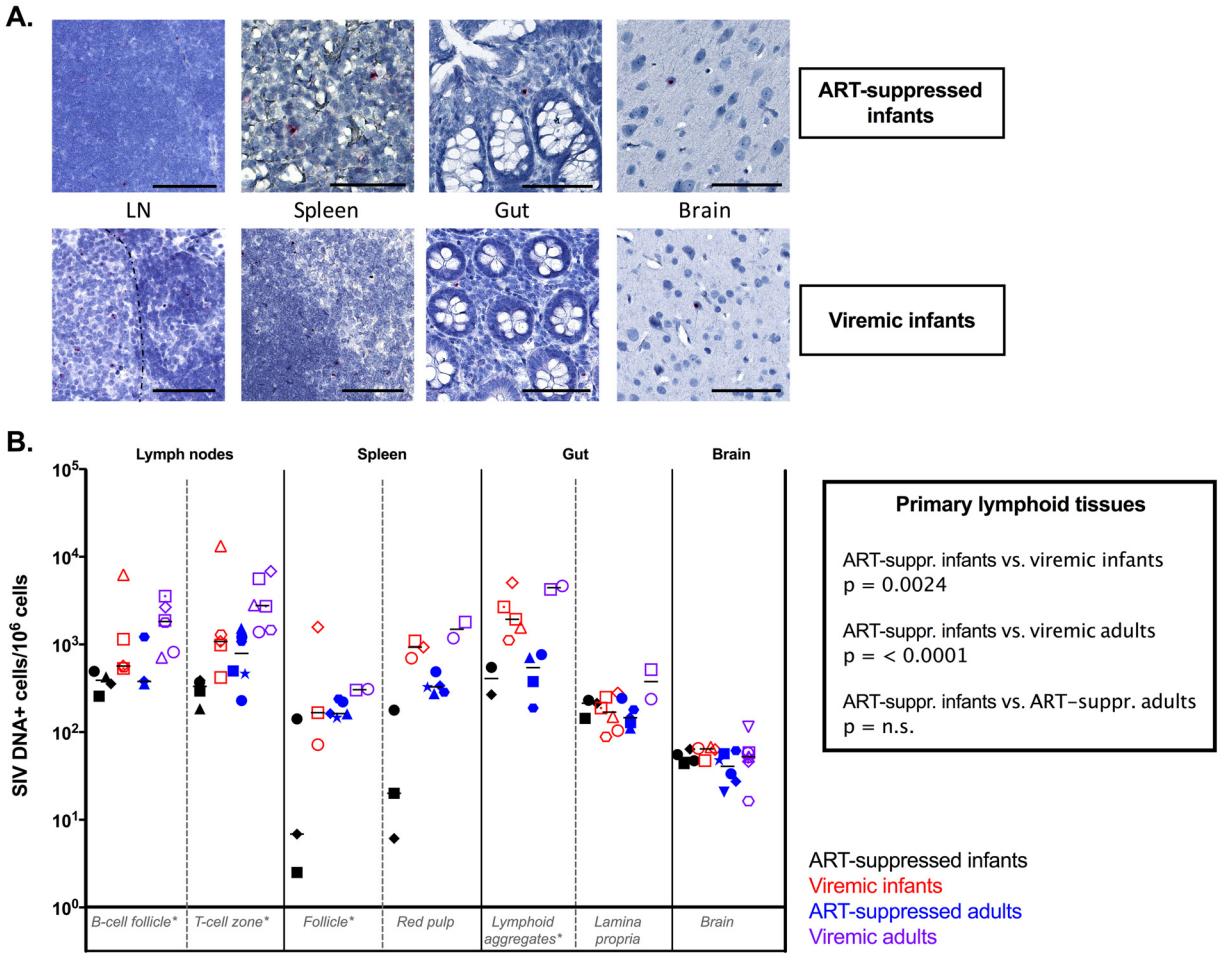

FIG 4 SIV DNA persistence in tissues. (A) Representative images of DNAscope *in situ* hybridization of ART-suppressed infant RMs (top) and viremic infant RMs (bottom). Bars, 50 μm. (B) Comparative analyses of SIV DNA levels measured by DNAscope in lymphoid tissues and brain in ART-suppressed infant RMs, viremic ART-naive infant RMs, ART-suppressed adult RMs, and ART-naive viremic adult RMs. The horizontal lines represent medians. *, primary lymphoid tissues.

follicular dendritic cell (FDC) network in gut lymphoid aggregates and B-cell follicles in LN and spleen. We observed a drastic diminution of the number of trapped virions in ART-suppressed infants compared to viremic infants in all the tissues assessed (Fig. 6C). However, free viruses were observed in the LN of one infant and in the spleens of two infants on suppressive ART.

SIV persistence in CD4$^+$ T cells. We first measured the level of SIV DNA in total CD4$^+$ T cells isolated from peripheral blood and found a 1.7 log reduction comparing pretreatment to posttreatment time points (Fig. 7A) ($P = 0.0499$). To better characterize the CD4$^+$ T cell reservoir in infants compared to adults, we next sorted naive, stem cell memory (SCM) (T_{SCM}), central/transitional memory (CM/TM) ($T_{CM/TM}$), and effector memory (EM) (T_{EM}) CD4$^+$ T cells by fluorescence-activated cell sorter (FACS) from peripheral blood. The levels of cell-associated SIV DNA were measured in these CD4$^+$ T cell subsets isolated from the four ART-suppressed infant RMs (cohort A) (Table 1), as well as four RM adults who received the same ART regimen for comparable periods (cohort E) (Table 1). In ART-suppressed RM infants, SIV DNA was detected at similar levels in naive and memory populations of CD4$^+$ T cells in the peripheral blood (Fig. 7B). However, in ART-suppressed RM adults, the frequency of SIV DNA in peripheral naive CD4$^+$ T cells was significantly lower than in SCM ($P = 0.0483$), CM ($P = 0.0092$), and TM ($P = 0.0199$) cells (Fig. 7B). Furthermore, the peripheral CD4$^+$ T cell pool was composed of a majority of naive CD4$^+$ T cells in infants (Fig. 7C), and naive CD4$^+$ T cells

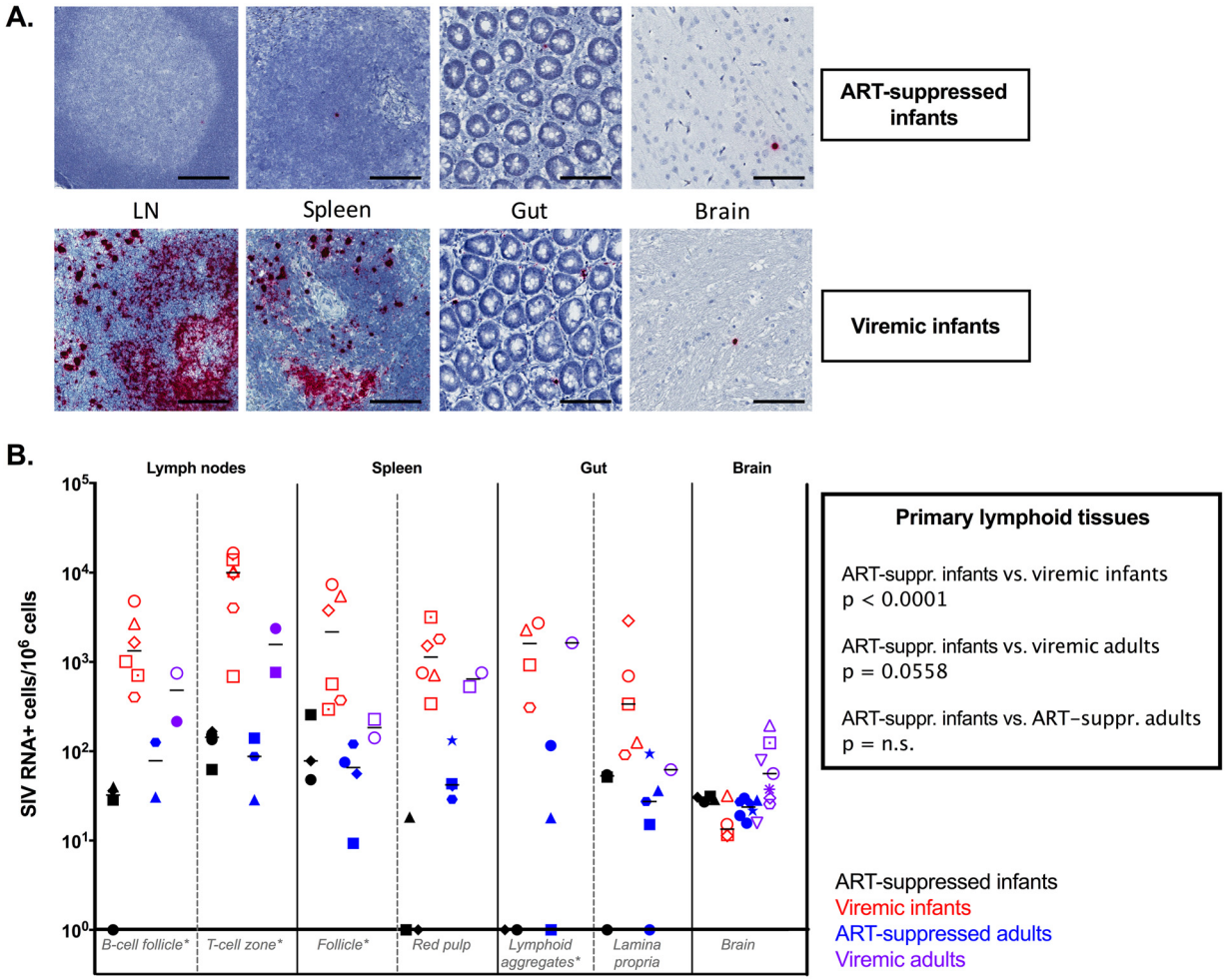

FIG 5 SIV RNA persistence in tissues. (A) Representative images of RNAscope *in situ* hybridization of ART-suppressed infant RMs (top) and viremic infant RMs (bottom). Bars, 50 μm. (B) Comparative analyses of SIV RNA levels measured by RNAscope in lymphoid tissues and brain in ART-suppressed infant RMs, viremic ART-naive infant RMs, ART-suppressed adult RMs, and ART-naive viremic adult RMs. The horizontal lines represent medians. *, primary lymphoid tissues.

were found to represent the main contributors to the total SIV reservoir in CD4$^+$ T cells in infants, with a relative contribution of 74% in the peripheral blood (Fig. 7D). As expected, naive CD4$^+$ T cells were less frequent in the peripheral blood of adults (Fig. 7C) and made a relative contribution of only 14% to the total CD4$^+$ T cell reservoir in blood (Fig. 7D). Conversely, the CM/TM subsets of CD4$^+$ T cells represented the largest contributors to the total SIV reservoir in adults at 65% (Fig. 7D).

We undertook a similar comparison in the lymph node compartment, where naive, SCM, CM/TM, and follicular helper (TFH) CD4$^+$ T cells were sorted from various LN, including superficial, mesenteric, and retroperitoneal LN. Cell-associated SIV DNA was detected at similar levels in all the populations of CD4$^+$ T cells in ART-suppressed infants, with slightly higher levels seen in TFH cells from superficial LN than in naive cells ($P = 0.0279$) (Fig. 8A). The distributions of the CD4$^+$ T cell pool (Fig. 8B) and the SIV reservoir (Fig. 8C) within LN CD4$^+$ T cell subsets were again different between SIV-infected, ART-suppressed infants and adults, with higher levels of naive CD4$^+$ T cells that made a greater contribution to the SIV reservoir in CD4$^+$ T cells in infants (range, 73 to 88% in infants compared to 42 to 57% in adults). Due to the increased frequency of naive T cells in the LN compared to peripheral blood of adults, the differential contribution of the naive subset to the LN CD4$^+$ T cell reservoir between adults and infants was less striking than in the blood (Fig. 7D and 8C).

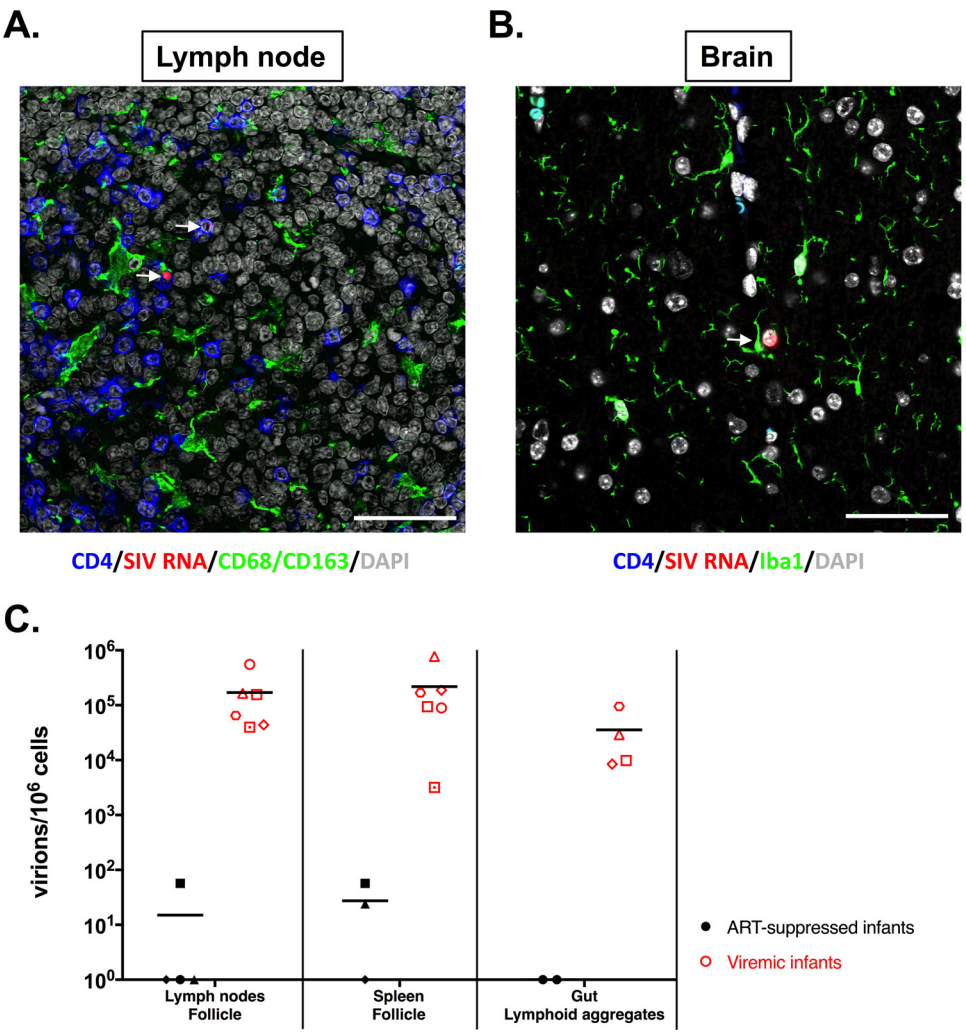

FIG 6 vRNA$^+$ cells in ART-suppressed infants. (A) Lymph nodes were stained, for all treated infants, for CD4, SIV RNA, CD68/CD163 (myeloid cells), and DAPI (4′,6-diamidino-2-phenylindole). (B) Brain sections were stained for CD4, SIV RNA, Iba1, and DAPI. The arrows indicate SIV-infected cells. The images are representative of three animals per tissue type. All the images are shown at ×60 magnification. All scale bars, 200 μm. (C) Comparative analysis of SIV virions persisting in the follicular dendritic cell network measured by RNAscope in primary lymphoid tissues in ART-suppressed infant RMs and viremic ART-naive infant RMs.

Having shown that SIV DNA persists in both naive and memory CD4$^+$ T cells of ART-suppressed infant RMs and that naive T cells appear to constitute a relatively large proportion of the CD4$^+$ T cell reservoir in infants, we next asked if these cells harbored replication-competent virus. It should first be noted that, based on both low to absent cell surface expression of activation markers and lack of gamma interferon (IFN-γ) production following *ex vivo* stimulation with phorbol myristate acetate (PMA)/ionomycin (Fig. 9A and B), the cells we identified and sorted as naive CD4$^+$ T cells displayed a phenotypic and functional profile expected of naive T cells. In two of four RM infants where sufficient cells were available, we used the gold standard quantitative viral outgrowth assay (QVOA) to measure replication-competent virus in naive and memory CD4$^+$ T cells isolated from LN. Replication-competent SIV was recovered from the naive and memory CD4$^+$ T cell compartments of both RM infants, with an estimated frequency of latently infected naive CD4$^+$ T cells of 0.8 to 1.1 per million cells and memory CD4$^+$ T cells of 0.8 to 5.6 per million cells (Fig. 9C). Acknowledging the small sample size, this result is suggestive of a previously unrecognized replication-competent naive CD4$^+$ T cell reservoir in infants.

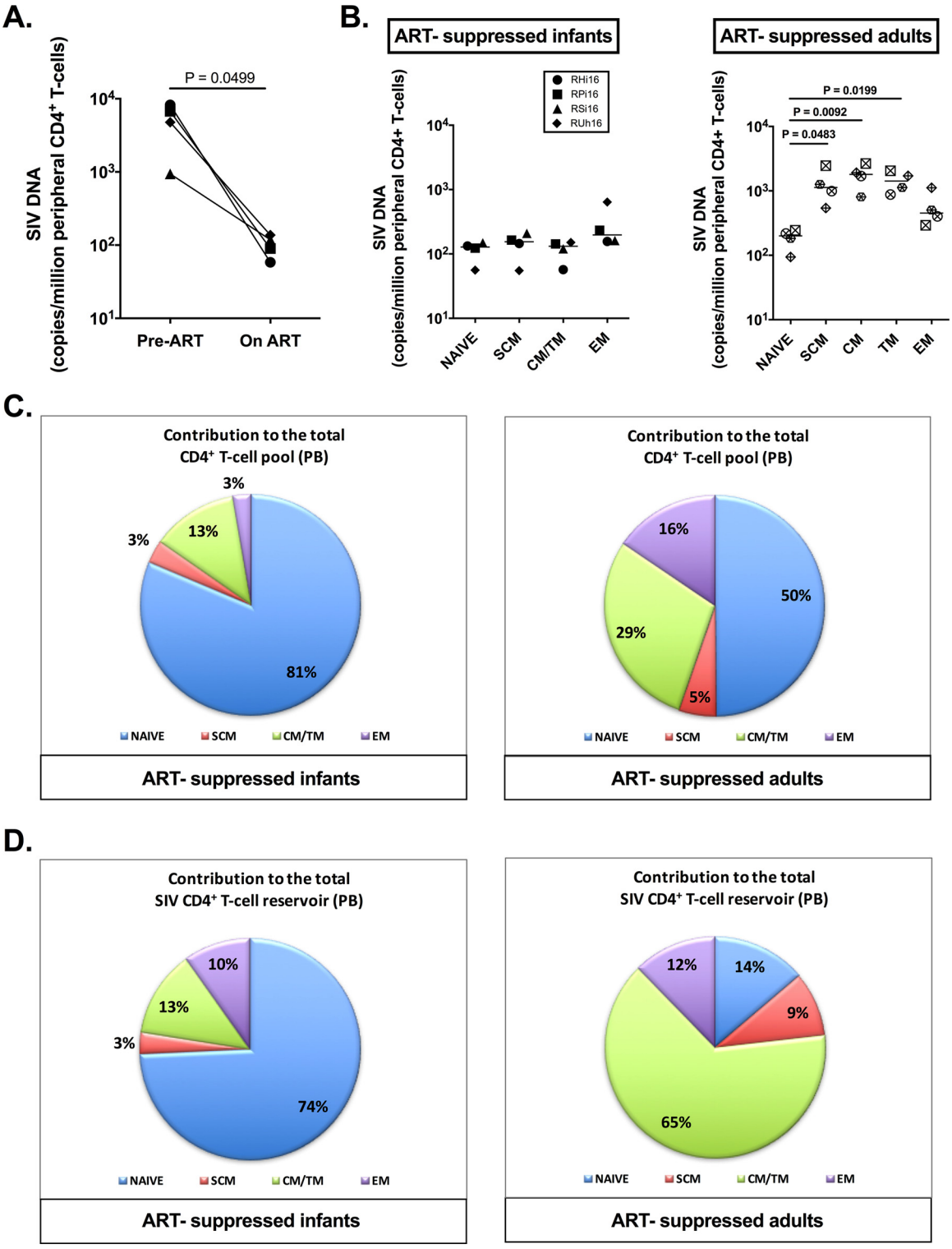

FIG 7 SIV DNA persistence in peripheral CD4+ T cells of ART-treated SIV-infected RM infants and adults. (A) Comparison of estimated SIV DNA levels in the peripheral CD4+ T cell DNA before (days 21 to 35 postinfection [p.i.]) and after (days 189 to 273 p.i.) ART in infant RMs calculated based on PBMC frequency of infection as determined by PCR and the frequency of CD4+ T cells in PBMCs as determined by flow cytometry. (B) On-ART SIV DNA levels in sorted subsets of peripheral CD4+ T cells (naive, SCM, CM/TM, and EM CD4+ T cells) as determined by PCR. The lines represent medians. (C) Relative contributions of CD4+ T cell subsets (naive, SCM, CM/TM, and EM CD4+ T cells) to the total peripheral CD4+ T cell pool. (D) Relative contribution of CD4+ T cell subsets (naive, SCM, CM/TM, and EM CD4+ T cells) to the total peripheral CD4+ T cell SIV reservoir.

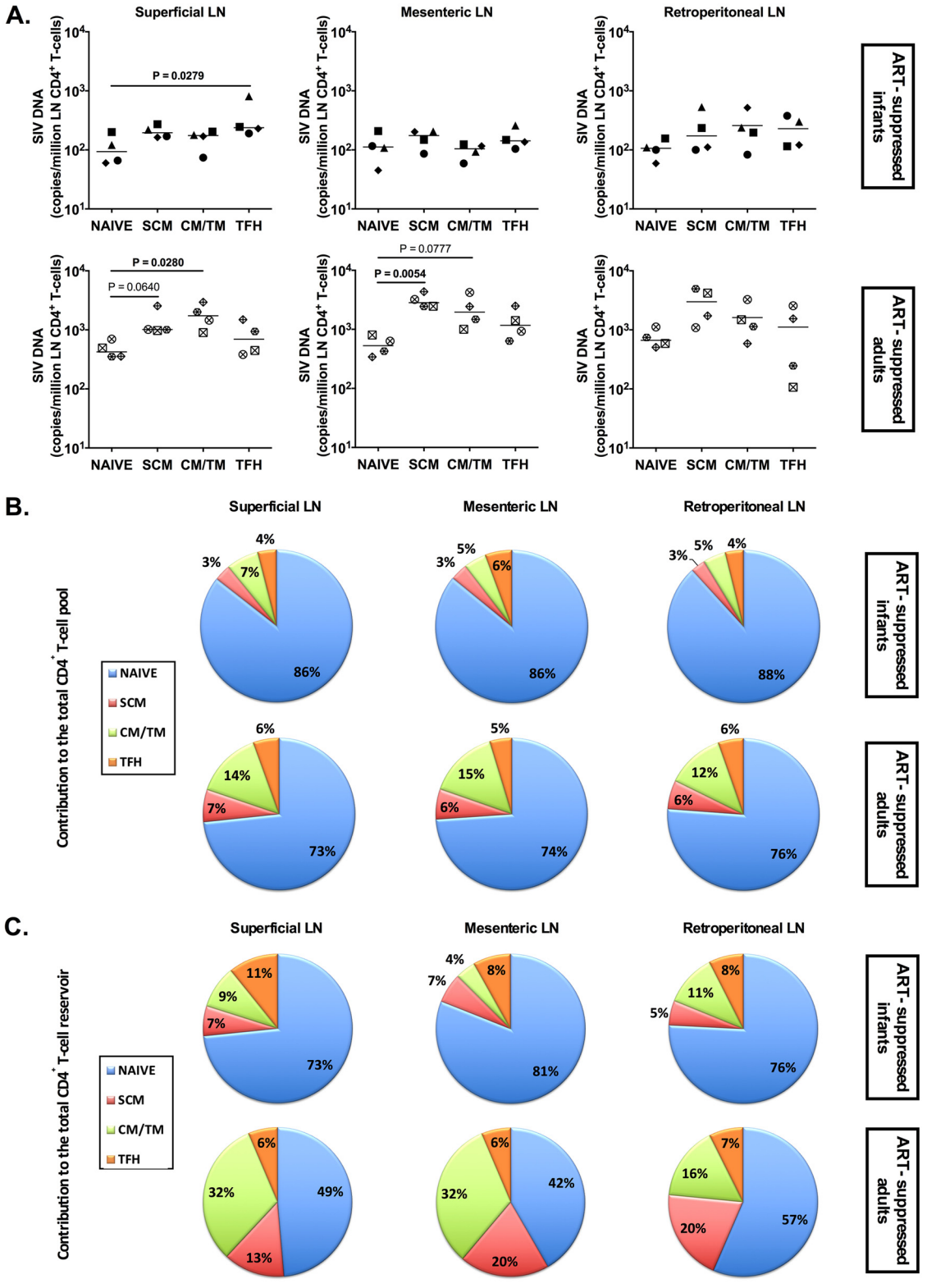

FIG 8 SIV DNA persistence in LN CD4$^+$ T cells of ART-treated SIV-infected RM infants and adults. (A) On-ART SIV DNA levels in subsets of CD4$^+$ T cells (naive, SCM, CM, and TFH CD4$^+$ T cells) sorted from superficial (axillary and inguinal), mesenteric, and retroperitoneal LN. The horizontal lines represent medians. (B) Relative contributions of CD4$^+$ T cell subsets (naive, SCM, CM/TM, and EM CD4$^+$ T cells) to the total LN CD4$^+$ T cell pool. (C) Relative contributions of CD4$^+$ T cell subsets (naive, SCM, CM/TM, and EM CD4$^+$ T cells) to the total LN CD4$^+$ T cell SIV reservoir.

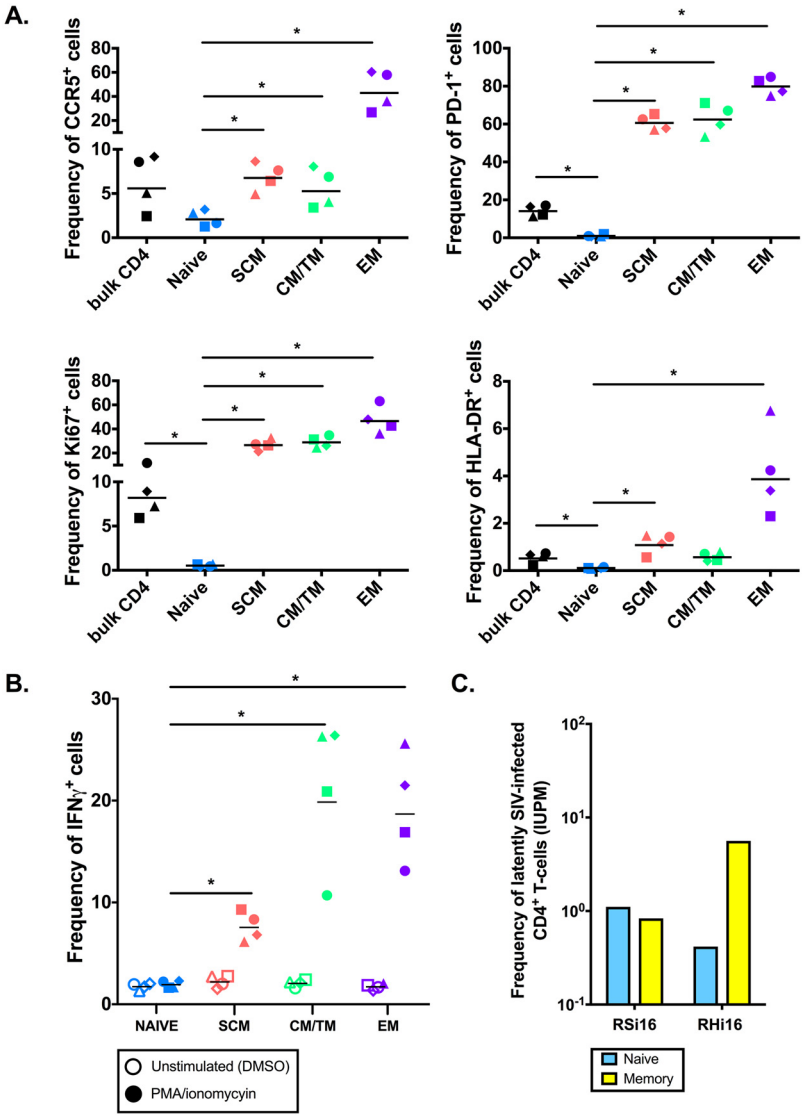

FIG 9 Characterization of the naive CD4$^+$ T cell reservoir in ART-treated SIV-infected RM infants. (A) Flow-cytometric assessment of CCR5, PD-1, Ki67, and HLA-DR expression at the surfaces of peripheral bulk, naive, SCM, CM/TM, and EM CD4$^+$ T cells. (B) Flow-cytometric analyses of IFN-γ expression on splenic naive, SCM, CM/TM, and EM CD4$^+$ T cells following *ex vivo* stimulation with PMA/ionomycin. *, $P < 0.05$. (C) Assessment of the frequencies of naive and memory CD4$^+$ T cells carrying replication-competent SIV in ART-suppressed RM infants by quantitative viral outgrowth assay.

DISCUSSION

This pilot study provides key insight into SIV persistence following oral infection in infants, highlighting specific anatomic and cellular contributors to the viral reservoir in this population. We demonstrate safety in administering ART in infant RMs for prolonged periods and efficient viral suppression by ART in SIV-infected RM infants with sustained undetectable plasma viral loads. The dynamics of infection and viral suppression were similar to those observed in HIV-infected children (24, 25) and led to a partial restoration of the peripheral level of CD4$^+$ T cells, as previously reported in ART-treated patients (33). SIV persistence after several months of ART was shown in various tissues, including blood, LN, spleen, gut, and brain.

As the half-life and homeostasis of the cells latently infected by HIV are critical in the maintenance of the viral reservoir over time, we specifically assessed SIV DNA persistence in naive and memory subsets of CD4$^+$ T cells defined based on their differentiation phenotypes. We found similar levels of infection in naive CD4$^+$ T cells and in the

SCM, CM/TM, and EM CD4$^+$ T cells in blood of ART-treated SIV-infected RM infants, with comparable findings in LN (with the exception of TFH cells showing an increased frequency of infection compared to naive cells in the superficial LN, but not mesenteric and retroperitoneal LN). These results differ from what we observed in ART-suppressed adult macaques and previous reports of ART-treated adult patients, in whom memory cells, especially TM and CM cells, have been shown to have the highest frequencies of HIV (12, 34). The prior work was performed in patients on long-term ART, while in our pilot study, ART duration was limited to 6 to 9 months, potentially contributing to the observed differences. However, we show here that in adult RMs who received the same ART regimen for a similar duration as the infants, the frequency of naive CD4$^+$ T cells harboring SIV DNA was significantly lower than in subsets of memory CD4$^+$ T cells, which is consistent with the human data. The overall frequency of memory CD4$^+$ T cell infection was higher in adult than in infant RMs, which may in part reflect the route of virus inoculation (intravenous versus oral); even so, the similar levels of persistent SIV DNA in naive and memory T cells of infants is notable.

HIV DNA is almost always detected in naive CD4$^+$ T cells in both viremic and ART-suppressed individuals, but how naive CD4$^+$ T cells become infected and their contribution to the latent reservoir are still sources of debate (35–38). Studies in ART-treated patients suggest that infection of naive CD4$^+$ T cells occurs primarily in the periphery rather than during maturation in the thymus (35, 36, 38). HIV/SIV coreceptor CCR5 expression on the surfaces of naive CD4$^+$ T cells is very low, and viral entry could involve alternative coreceptors, such as CXCR4 in humans or CXCR6 and GPR15 in monkeys (39, 40). However, both SIV_{mac251}, used in this study, and SIV_{mac239} have been shown to exclusively use CCR5 for entry into rhesus macaque CD4$^+$ T cells (41, 42). The lymphoid tissue microenvironment may also have an important role in HIV infection of naive T cells, with increased susceptibility to infection in tonsil lymphoid tissue compared to purified CD4$^+$ T cells alone (43, 44). In our model of pediatric infection, naive CD4$^+$ T cells appeared to be the main contributors to the CD4$^+$ T cell SIV reservoir and contained quantifiable replication-competent virus, suggesting that these cells might be of critical importance in HIV persistence in infants. Given the robust naive CD4$^+$ T cell compartment during the period of infancy, this finding requires increased attention and further investigation into the mechanisms of reservoir establishment and maintenance in these cells. A greater focus on the latent reservoir in naive CD4$^+$ T cells may be warranted when developing cure strategies for the pediatric population.

DNAscope and RNAscope *in situ* hybridization showed viral persistence in lymphoid and nonlymphoid tissues of ART-suppressed RM infants, with levels similar to those in ART-suppressed RM adults. While a reduction of virus levels was observed in primary lymphoid tissues in ART-suppressed compared to viremic RM infants, similar numbers of cells carrying SIV DNA or RNA were found in the brains of ART-suppressed and viremic RM infants, and vRNA$^+$ cells appeared to be of myeloid origin. In line with this result, low to undetectable levels of the ART drugs used were found in the RM infant brains at necropsy. It should be emphasized that levels of SIV RNA and DNA in the brain were low, but this anatomic site is increasingly recognized as a latent reservoir for which unique approaches may be needed to eliminate persistent virus (45–47). Consistent with a recent report, similar levels of vDNA$^+$ cells were also found in the gut lamina propria of the ART-suppressed and viremic infant RMs (46).

As this study was designed to establish the utility of the SIV-infected infant RM model for investigations of viral reservoirs under ART in a pediatric setting, there are a number of limitations (animal numbers, ART duration, cross-sectional analysis, and heterogeneity of measurements between animals) that prevent us from reaching overarching conclusions from our findings. However, given the difficulties of studying HIV reservoirs in children, the establishment of this experimental model is of major importance, with the findings here providing key insights into differences between infant and adult RMs.

In conclusion, we have established a pediatric model of HIV suppression on ART recapitulating the key features of HIV persistence in humans. Following ART initiation,

sustained undetectable plasma viral loads were maintained, with reduction in SIV RNA and DNA in lymphoid tissues but stable levels of SIV RNA and DNA in the brain. Naive $CD4^+$ T cells constituted a large component of the total CD4 reservoir in blood and LN of ART-suppressed RM infants, a finding that was not seen in adults. These results reveal important aspects of HIV/SIV persistence in infants and provide insight into strategic targets for cure interventions in a pediatric population. This model can be used as an experimental *in vivo* platform to test emerging cure interventions being developed for infants and children.

MATERIALS AND METHODS

Animals and infection. Four infant Indian RMs (*Macaca mulatta*), with exclusion of Mamu B*08- and B*17-positive animals, were enrolled in this study. The animals were born at the Yerkes National Primate Research Center (YNPRC) to dams housed in indoor/outdoor group housing. The infants were removed from the dams when they were approximately 3 months old and transferred to a nursery, where they were housed in social pairs with either full contact or protected contact for the duration of the study. The infants were fed standard primate jumbo chow biscuits (Jumbo Monkey Diet 5037; Purina Mills, St. Louis, MO) based on age and weight in accordance with YNPRC standard operating procedures (SOPs) for nonhuman primate (NHP) feeding. The animals also received enrichment of fresh produce daily. The animals were orally infected at 20 to 21 weeks of age with two consecutive doses of 10^5 $TCID_{50}$ of SIV_{mac251}. All the animals were treated in accordance with Emory University and Yerkes National Primate Research Center Institutional Animal Care and Use Committee regulations. An additional four groups of rhesus macaques were used for cross-sectional comparative analyses (Table 1). The infants in cohort B were housed at the Washington National Primate Research Center and were orally infected between 10 and 16 weeks of age with 10^3 to 10^4 $TCID_{50}$ of SIV_{mac251}. The adult rhesus macaques were housed at YNPRC and were infected with SIV_{mac239} or SIV_{mac251} (48).

Antiretroviral therapy. The four RM infants were treated with a potent three-drug ART regimen initiated 35 days postinfection. The preformulated ART cocktail contained two reverse transcriptase inhibitors, 20 mg/kg PMPA and 40 mg/kg FTC, plus 2.5 mg/kg of the integrase inhibitor DTG. This ART cocktail was administered once daily at 1 ml/kg via the subcutaneous route.

Sample collection and processing. Blood samples were collected regularly and used for a complete blood count, routine chemical analysis, and immunostaining, with plasma separated by centrifugation within 1 h of phlebotomy. PBMCs were prepared by density gradient centrifugation. Tissue samples, including gut, brain, spleen, tonsils, and LN, were collected postmortem. After two washes in RPMI and removal of connective and fat tissues, gut tissues were cut in small pieces and LN and tonsils were ground using a 70-μm cell strainer. Gut cells were isolated by digestion with collagenase and DNase I for 2 h at 37°C and then passed through a 70-μm cell strainer. The cell suspensions obtained were washed and immediately used for immunostaining or cryopreserved at −80°C until use.

Antiretroviral drug measurements. (i) Mass spectrometry imaging. The spatial distribution of ARV drug levels was measured by infrared matrix-assisted laser desorption-electrospray ionization (26). Sections of tissue samples (10 μm) were prepared in a cryotome, thaw mounted on glass microscope slides, and maintained at −10°C on the sample stage of the IR-MALDESI source chamber prior to analysis. The stage translated the sample stepwise across the focused beam of an IR laser (IR-Opolette 2371; Opotek, Carlsbad, CA, USA), which desorbed sample material from adjacent 100-μm-diameter sampling locations. An electrospray ionized the desorbed neutral molecules, and the resulting ions were sampled into a high-resolving-power Thermo Fisher Scientific Q Exactive Plus (Bremen, Germany) mass spectrometer for synchronized analysis. Calibration of the IR-MALDESI response was performed on matching tissue from untreated RMs. To generate images from mass spectrometry data, raw data from each voxel was converted to the mzXML format using MSConvert software. These mzXML files were interrogated using free software developed for processing mass spectrometry imaging (MSI) data.

(ii) LC-MS/MS. Plasma, CSF, and PBMC pellet samples were extracted by protein precipitation with stable isotopically labeled internal standards. Serial 10-μm tissue sections were homogenized in 1 ml of 70:30 acetonitrile-1 mM ammonium phosphate (pH 7.4) using a Precellys 24 tissue homogenizer (Bertin Technologies, Montigny-le-Bretonneux, France). All analyses were conducted using a Shimadzu high-performance liquid chromatography (HPLC) system for chromatographic separation and an AB Sciex API 5000 mass spectrometer (AB Sciex, Foster City, CA, USA) equipped with a turbospray interface for detection using validated LC-MS/MS assays. The samples were analyzed with a set of calibration standards (0.01 to 50 ng/ml) and quality control (QC) samples. The precision and accuracy of the calibration standards and QC samples met the acceptance criteria (PMPA and FTC, 15%; PMPAdp and FTCtp, 20%; DTG, 35%).

RNAscope and DNAscope analyses. We utilized a novel next-generation, ultrasensitive *in situ* hybridization technology for the detection of both SIV RNA (RNAscope) and DNA (DNAscope) with quantitative image analysis as previously described (32, 46). Regions of interest (0.25 mm^2) were selected to maximize the size of the tissue to be assessed. The average total numbers of cells assessed were 138,461 for the spleen, 111,394 for the LN, 88,461 for the gut, and 286,497 for the brain.

Immunophenotype by flow cytometry. Multicolor flow cytometric analysis was performed on whole blood or cell suspensions using predetermined optimal concentrations of the following fluorescently conjugated monoclonal antibodies (MAbs): CD3-allophycocyanin (APC)-Cy7 (clone SP34-2), CD95-phycoerythrin (PE)-Cy5 (clone DX2), Ki67-AF700 (clone B56), HLA-DR-peridinin chlorophyll protein

(PerCP)-Cy5.5 (clone G46-6), CCR7-fluorescein isothiocyanate (FITC) (clone 150503), CCR5-APC (clone 3A9), and CD45RA-PE-Cy7 (clone L48) from BD Biosciences; CD8-BV711 (clone RPA-T8), CD4-BV650 (clone OKT4), and PD-1-BV421 (clone EH12.2H7) from BioLegend; and CD28-ECD (clone CD28-2) from Beckman-Coulter. Flow cytometric acquisition and analysis of samples were performed on at least 100,000 events on an LSR II flow cytometer driven by the FACSDiva software package (BD Biosciences). Analyses of the acquired data were performed using FlowJo version 10.0.4 software (TreeStar).

Cell sorting. Prior to sorting, peripheral $CD4^+$ T cells were enriched with the use of magnetic beads and column purification (Miltenyi Biotec). Enriched peripheral $CD4^+$ T cells, lymph nodes, or spleen cell suspensions were then stained with previously determined volumes of the following fluorescently conjugated MAbs: CD3-APC-Cy7 or -AF700 (clone SP34-2), CCR7-PE-Cy7 (clone 3D12), CD8-APC-Cy7 (clone SK1), CD45RA-APC (clone 5H9), and CD95-PE-Cy5 (clone DX2) from BD Bioscience; CD28-ECD (clone CD28.2) from Beckman Coulter; and CD4-BrilliantViolet650 (clone OKT4) and CD8-BV421 (clone RPA-T8) from BioLegend. Populations for sorting were defined as follows: naive cells, $CD45RA^+$ $CCR7^+$ $CD95^-$; T_{SCM} cells, $CD45RA^+$ $CCR7^+$ $CD95^+$ $CD28^+$; $T_{CM/TM}$ cells, $CD45RA^-$ $CD95^+$ $CCR7^+$; and T_{EM} cells, $CD95^+$ $CCR7^-$. LN cell suspensions were stained with the same antibodies and CXCR5-PE (clone MU5UBEE) from eBioscience and PD-1-BV421 (clone EH12.2H7) from BioLegend to define TFH cells. TFH cells were defined as $CXCR5^{hi}$ $PD\text{-}1^{high}$. Memory $CD4^+$ T cells were defined as follows: $CD45RA^-$ $CD95^+$. Sorting was performed on a FACSAria LSR II (BD Biosciences) equipped with FACS Diva software.

Plasma RNA and cell-associated DNA viral quantification. Plasma viral quantification was performed as described previously. Frozen cell pellets were lysed with proteinase K (100 μg/ml in 10 mM Tris-HCl, pH 8) for 1 h at 56°C. Quantification of SIV_{mac} *gag* DNA was performed by quantitative PCR using a 5′ nuclease (TaqMan) assay with an ABI7500 system (PerkinElmer Life Sciences). The sequence of the forward primer for SIV_{mac} *gag* was 5′-GAAGGTGAAGGTCGGAGTC-3′, the reverse primer sequence was 5′-GAAGATGGTGATGGGATTTC-3′, and the probe sequence was 5′-6-carboxyfluorescein (FAM)-CAAGCTTCCCGTTCTCAGCC-6-carboxytetramethylrhodamine (TAMRA)-3′. Cell lysate (7.5 μl) was mixed in a 50-μl reaction mixture containing 1× platinum buffer, 3.5 mM $MgCl_2$, 0.2 mM deoxynucleoside triphosphate (dNTP), 200 nM primers, 150 nM probe, and 2 U Platinum Taq. For cell quantification, quantitative PCR was performed simultaneously for the monkey albumin gene copy number. The sequence of the forward (F) primer for albumin was 5′-TGCATGAGAAAACGCCAGTAA-3′; the reverse primer sequence was 5′-ATGGTCGCCTGTTCACCAA-3′, and the probe sequence was 5′-AGAAAGTCACCAAATGCTGCACGGAATC-3′ (49). The reactions were performed on a 7500 real-time PCR system (Applied Biosystems) with the following thermal program: 5 min at 95°C, followed by 40 cycles of denaturation at 95°C for 15 s and annealing at 60°C for 1 min.

Ex vivo IFN-γ production. Cryopreserved splenocytes were stimulated with PMA (50 ng/ml) and ionomycin (1 μg/ml) for 4 h in the presence of monensin (BD GolgiStop protein transport inhibitor; BD Bioscience) or with dimethyl sulfoxide (DMSO). The cells were then stained with the Abs listed in "Cell sorting" above and with IFN-γ–PE (clone B27) from BD Bioscience following cell permeabilization.

SIV quantitative viral outgrowth assay. Latently infected cells were quantified using a limiting-dilution culture assay in which naive and memory $CD4^+$ T cells sorted from the LN of 2 ART-suppressed infant RMs were cocultured with CEMx174 cells in duplicate 5-fold serial dilutions ranging from as many as 1×10^6 cells per well to as few as 320 cells per well. The cells were cultured in RPMI medium containing 10% fetal bovine serum, 4 mM L-glutamine, 50 U/ml penicillin, 50 μg/ml streptomycin, and 100 U/ml interleukin 2 (IL-2) (Sigma). The ratio of target cells added was 4:1 for the 2 highest dilutions. A constant number (50,000) of CEMx174 cells were added to all the other wells. The cultures were split every 2 or 3 days, and fresh medium was added. After 28 days, growth of virus was detected by quantitative reverse transcription (qRT)-PCR. SIV RNA was isolated from 1,250 μl of culture supernatant using a Zymo viral RNA isolation kit (Zymo Research). The cell culture supernatant underwent centrifugation for 90 min at 21,000 × *g* before extraction, following the manufacturer's instructions. DNase treatment was performed using an RQ1 RNase-free DNase kit (Promega). A one-step qRT-PCR targeting SIV *gag* was performed using an Applied Biosystems 7500 real-time PCR system (Applied Biosystems) and Veriquest Probe one-step qRT-PCR master mix (Affimetrix) with the following primers and probe: SIVgagFwd, 5′-GCAGAGGAGGAAATTACCCAGTAC-3′; SIVgagRev, 5′-CAATTTTACCCAGGCATTTAATGTT-3′; SIVgag-probe, 5′-FAM-TGTCCACCTGCCATTAAGCCCGA-3IBFQ-3′. The frequencies of infected cells were determined by the maximum-likelihood method (50) and were expressed as infectious units per million (IUPM) $CD4^+$ T cells.

Statistical analyses. Repeated-measures analyses of peripheral $CD4^+$ T cell counts were performed with a means model via the SAS MIXED procedure (version 9.4), providing separate estimates of the means by week postinfection. A compound-symmetric variance-covariance form in repeated measurements was assumed for the $CD4^+$ T cell count, and robust estimates of the standard errors of parameters were used to perform statistical tests and to construct 95% confidence intervals (51). The model-based means are unbiased by unbalanced and missing data, as long as the missing data are noninformative (missing at random). To compare $CD4^+$ T cell counts at different periods, specific statistical tests (paired *t* tests) were done within the framework of the mixed-effects linear model. For the cross-sectional analysis of SIV RNA^+ and DNA^+ cell levels between cohorts as measured by RNAscope and DNAscope, the nonparametric Kruskal-Wallis test with Dunn's correction for multiple comparisons was used. To analyze SIV DNA levels in naive and memory $CD4^+$ T cell subsets, we used the nonparametric Kruskal-Wallis test with Dunn's correction for multiple comparisons, with naive T cell values as the control comparison.

ACKNOWLEDGMENTS

We thank Gilead for provision of the antiretroviral drugs PMPA and FTC.

This work was supported in part with federal funds from the National Cancer Institute (NIH contract HHSN261200800001E). The study was funded by the Emory+Children's Pediatric Center Seed Grant Program, the Campbell Family Foundation, and R01-AI133706 (all to A.C.) and by R01-DE023047 (to D.L.S.). We also acknowledge support from the Yerkes National Primate Research Center (RR000165/OD011132) and the Emory Center for AIDS Research (P30 AI050409).

The content of this publication does not necessarily reflect the views or policies of the Department of Health and Human Services, nor does mention of trade names, commercial products, or organizations imply endorsement by the U.S. government.

REFERENCES

1. Barnhart HX, Caldwell MB, Thomas P, Mascola L, Ortiz I, Hsu HW, Schulte J, Parrott R, Maldonado Y, Byers R. 1996. Natural history of human immunodeficiency virus disease in perinatally infected children: an analysis from the Pediatric Spectrum of Disease Project. Pediatrics 97:710–716.
2. Newell ML, Coovadia H, Cortina-Borja M, Rollins N, Gaillard P, Dabis F, Ghent International AIDS Society (IAS) Working Group on HIV Infection in Women and Children. 2004. Mortality of infected and uninfected infants born to HIV-infected mothers in Africa: a pooled analysis. Lancet 364:1236–1243. https://doi.org/10.1016/S0140-6736(04)17140-7.
3. Richardson BA, Mbori-Ngacha D, Lavreys L, John-Stewart GC, Nduati R, Panteleeff DD, Emery S, Kreiss JK, Overbaugh J. 2003. Comparison of human immunodeficiency virus type 1 viral loads in Kenyan women, men, and infants during primary and early infection. J Virol 77:7120–7123. https://doi.org/10.1128/JVI.77.12.7120-7123.2003.
4. Shearer WT, Quinn TC, LaRussa P, Lew JF, Mofenson L, Almy S, Rich K, Handelsman E, Diaz C, Pagano M, Smeriglio V, Kalish LA. 1997. Viral load and disease progression in infants infected with human immunodeficiency virus type 1. Women and Infants Transmission Study Group. N Engl J Med 336:1337–1342.
5. Luzuriaga K, Gay H, Ziemniak C, Sanborn KB, Somasundaran M, Rainwater-Lovett K, Mellors JW, Rosenbloom D, Persaud D. 2015. Viremic relapse after HIV-1 remission in a perinatally infected child. N Engl J Med 372:786–788. https://doi.org/10.1056/NEJMc1413931.
6. Persaud D, Gay H, Ziemniak C, Chen YH, Piatak M, Jr, Chun TW, Strain M, Richman D, Luzuriaga K. 2013. Absence of detectable HIV-1 viremia after treatment cessation in an infant. N Engl J Med 369:1828–1835. https://doi.org/10.1056/NEJMoa1302976.
7. Bitnun A, Samson L, Chun TW, Kakkar F, Brophy J, Murray D, Justement S, Soudeyns H, Ostrowski M, Mujib S, Harrigan PR, Kim J, Sandstrom P, Read SE. 2014. Early initiation of combination antiretroviral therapy in HIV-1-infected newborns can achieve sustained virologic suppression with low frequency of CD4+ T cells carrying HIV in peripheral blood. Clin Infect Dis 59:1012–1019. https://doi.org/10.1093/cid/ciu432.
8. Butler KM, Gavin P, Coughlan S, Rochford A, McDonagh S, Cunningham O, Poulsom H, Watters SA, Klein N. 2015. Rapid viral rebound after 4 years of suppressive therapy in a seronegative HIV-1 infected infant treated from birth. Pediatr Infect Dis J 34:e48–e51. https://doi.org/10.1097/INF.0000000000000570.
9. Frange P, Faye A, Avettand-Fenoel V, Bellaton E, Descamps D, Angin M, David A, Caillat-Zucman S, Peytavin G, Dollfus C, Le Chenadec J, Warszawski J, Rouzioux C, Saez-Cirion A, ANRS EPF-CO10 Pediatric Cohort, ANRS EP47 VISCONTI Study Group. 2016. HIV-1 virological remission lasting more than 12 years after interruption of early antiretroviral therapy in a perinatally infected teenager enrolled in the French ANRS EPF-CO10 paediatric cohort: a case report. Lancet HIV 3:e49–e54. https://doi.org/10.1016/S2352-3018(15)00232-5.
10. Giacomet V, Trabattoni D, Zanchetta N, Biasin M, Gismondo M, Clerici M, Zuccotti G. 2014. No cure of HIV infection in a child despite early treatment and apparent viral clearance. Lancet 384:1320. https://doi.org/10.1016/S0140-6736(14)61405-7.
11. Luzuriaga K, Mofenson LM. 2016. Challenges in the elimination of pediatric HIV-1 infection. N Engl J Med 374:761–770. https://doi.org/10.1056/NEJMra1505256.
12. Chomont N, El-Far M, Ancuta P, Trautmann L, Procopio FA, Yassine-Diab B, Boucher G, Boulassel MR, Ghattas G, Brenchley JM, Schacker TW, Hill BJ, Douek DC, Routy JP, Haddad EK, Sekaly RP. 2009. HIV reservoir size and persistence are driven by T cell survival and homeostatic proliferation. Nat Med 15:893–900. https://doi.org/10.1038/nm.1972.
13. Chun TW, Carruth L, Finzi D, Shen X, DiGiuseppe JA, Taylor H, Hermankova M, Chadwick K, Margolick J, Quinn TC, Kuo YH, Brookmeyer R, Zeiger MA, Barditch-Crovo P, Siliciano RF. 1997. Quantification of latent tissue reservoirs and total body viral load in HIV-1 infection. Nature 387:183–188. https://doi.org/10.1038/387183a0.
14. Finzi D, Hermankova M, Pierson T, Carruth LM, Buck C, Chaisson RE, Quinn TC, Chadwick K, Margolick J, Brookmeyer R, Gallant J, Markowitz M, Ho DD, Richman DD, Siliciano RF. 1997. Identification of a reservoir for HIV-1 in patients on highly active antiretroviral therapy. Science 278:1295–1300. https://doi.org/10.1126/science.278.5341.1295.
15. Wong JK, Hezareh M, Gunthard HF, Havlir DV, Ignacio CC, Spina CA, Richman DD. 1997. Recovery of replication-competent HIV despite prolonged suppression of plasma viremia. Science 278:1291–1295. https://doi.org/10.1126/science.278.5341.1291.
16. Del Prete GQ, Smedley J, Macallister R, Jones GS, Li B, Hattersley J, Zheng J, Piatak M, Jr, Keele BF, Hesselgesser J, Geleziunas R, Lifson JD. 2016. Comparative evaluation of coformulated injectable combination antiretroviral therapy regimens in simian immunodeficiency virus-infected rhesus macaques. AIDS Res Hum Retroviruses 32:163–168. https://doi.org/10.1089/aid.2015.0130.
17. Micci L, Ryan ES, Fromentin R, Bosinger SE, Harper JL, He T, Paganini S, Easley KA, Chahroudi A, Benne C, Gumber S, McGary CS, Rogers KA, Deleage C, Lucero C, Byrareddy SN, Apetrei C, Estes JD, Lifson JD, Piatak M, Jr, Chomont N, Villinger F, Silvestri G, Brenchley JM, Paiardini M. 2015. Interleukin-21 combined with ART reduces inflammation and viral reservoir in SIV-infected macaques. J Clin Invest 125:4497–4513. https://doi.org/10.1172/JCI81400.
18. Shytaj IL, Norelli S, Chirullo B, Della Corte A, Collins M, Yalley-Ogunro J, Greenhouse J, Iraci N, Acosta EP, Barreca ML, Lewis MG, Savarino A. 2012. A highly intensified ART regimen induces long-term viral suppression and restriction of the viral reservoir in a simian AIDS model. PLoS Pathog 8:e1002774. https://doi.org/10.1371/journal.ppat.1002774.
19. Whitney JB, Hill AL, Sanisetty S, Penaloza-MacMaster P, Liu J, Shetty M, Parenteau L, Cabral C, Shields J, Blackmore S, Smith JY, Brinkman AL, Peter LE, Mathew SI, Smith KM, Borducchi EN, Rosenbloom DI, Lewis MG, Hattersley J, Li B, Hesselgesser J, Geleziunas R, Robb ML, Kim JH, Michael NL, Barouch DH. 2014. Rapid seeding of the viral reservoir prior to SIV viraemia in rhesus monkeys. Nature 512:74–77. https://doi.org/10.1038/nature13594.
20. Creek TL, Sherman GG, Nkengasong J, Lu L, Finkbeiner T, Fowler MG, Rivadeneira E, Shaffer N. 2007. Infant human immunodeficiency virus diagnosis in resource-limited settings: issues, technologies, and country experiences. Am J Obstet Gynecol 197:S64–S71.
21. Essajee S, Bhairavabhotla R, Penazzato M, Kiragu K, Jani I, Carmona S, Rewari B, Kiyaga C, Nkengasong J, Peter T. 2017. Scale-up of early infant HIV diagnosis and improving access to pediatric HIV care in global plan countries: past and future perspectives. J Acquir Immune Defic Syndr 75(Suppl 1):S51–S58. https://doi.org/10.1097/QAI.0000000000001319.
22. Seidenberg P, Nicholson S, Schaefer M, Semrau K, Bweupe M, Masese N, Bonawitz R, Chitembo L, Goggin C, Thea DM. 2012. Early infant diagnosis of HIV infection in Zambia through mobile phone texting of blood test

results. Bull World Health Organ 90:348–356. https://doi.org/10.2471/BLT.11.100032.
23. Cartwright EK, Palesch D, Mavigner M, Paiardini M, Chahroudi A, Silvestri G. 2016. Initiation of antiretroviral therapy restores CD4+ T memory stem cell homeostasis in simian immunodeficiency virus-infected macaques. J Virol 90:6699–6708. https://doi.org/10.1128/JVI.00492-16.
24. Chadwick EG, Capparelli EV, Yogev R, Pinto JA, Robbins B, Rodman JH, Chen J, Palumbo P, Serchuck L, Smith E, Hughes M, P1030 Team. 2008. Pharmacokinetics, safety and efficacy of lopinavir/ritonavir in infants less than 6 months of age: 24 week results. AIDS 22:249–255. https://doi.org/10.1097/QAD.0b013e3282f2be1d.
25. Chadwick EG, Pinto J, Yogev R, Alvero CG, Hughes MD, Palumbo P, Robbins B, Hazra R, Serchuck L, Heckman BE, Purdue L, Browning R, Luzuriaga K, Rodman J, Capparelli E, International Maternal Pediatric Adolescent Clinical Trials Group (IMPAACT) P1030 Team. 2009. Early initiation of lopinavir/ritonavir in infants less than 6 weeks of age: pharmacokinetics and 24-week safety and efficacy. Pediatr Infect Dis J 28:215–219. https://doi.org/10.1097/INF.0b013e31818cc053.
26. Thompson CG, Bokhart MT, Sykes C, Adamson L, Fedoriw Y, Luciw PA, Muddiman DC, Kashuba AD, Rosen EP. 2015. Mass spectrometry imaging reveals heterogeneous efavirenz distribution within putative HIV reservoirs. Antimicrob Agents Chemother 59:2944–2948. https://doi.org/10.1128/AAC.04952-14.
27. Wiznia A, Alvero C, Fenton T, George K, Townley E, Hazra R, Graham B, Buchanan A, Vavro C, Viani R. 2016. IMPAACT 1093: dolutegravir in 6- to 12-year-old HIV-infected children: 48-week results, abstr 816. Conf Retroviruses Opportunistic Infect, 22 to 25 February 2016, Boston, MA.
28. Baheti G, King JR, Acosta EP, Fletcher CV. 2013. Age-related differences in plasma and intracellular tenofovir concentrations in HIV-1-infected children, adolescents and adults. AIDS 27:221–225. https://doi.org/10.1097/QAD.0b013e32835a9a2d.
29. Wang LH, Wiznia AA, Rathore MH, Chittick GE, Bakshi SS, Emmanuel PJ, Flynn PM. 2004. Pharmacokinetics and safety of single oral doses of emtricitabine in human immunodeficiency virus-infected children. Antimicrob Agents Chemother 48:183–191. https://doi.org/10.1128/AAC.48.1.183-191.2004.
30. Dickinson L, Yapa HM, Jackson A, Moyle G, Else L, Amara A, Khoo S, Back D, Karolia Z, Higgs C, Boffito M. 2015. Plasma tenofovir, emtricitabine, and rilpivirine and intracellular tenofovir diphosphate and emtricitabine triphosphate pharmacokinetics following drug intake cessation. Antimicrob Agents Chemother 59:6080–6086. https://doi.org/10.1128/AAC.01441-15.
31. Wang LH, Begley J, St Claire RL III, Harris J, Wakeford C, Rousseau FS. 2004. Pharmacokinetic and pharmacodynamic characteristics of emtricitabine support its once daily dosing for the treatment of HIV infection. AIDS Res Hum Retroviruses 20:1173–1182. https://doi.org/10.1089/aid.2004.20.1173.
32. Deleage C, Wietgrefe SW, Del Prete G, Morcock DR, Hao XP, Piatak M, Jr, Bess J, Anderson JL, Perkey KE, Reilly C, McCune JM, Haase AT, Lifson JD, Schacker TW, Estes JD. 2016. Defining HIV and SIV reservoirs in lymphoid tissues. Pathog Immun 1:68–106. https://doi.org/10.20411/pai.v1i1.100.
33. Battegay M, Nuesch R, Hirschel B, Kaufmann GR. 2006. Immunological recovery and antiretroviral therapy in HIV-1 infection. Lancet Infect Dis 6:280–287. https://doi.org/10.1016/S1473-3099(06)70463-7.
34. Soriano-Sarabia N, Bateson RE, Dahl NP, Crooks AM, Kuruc JD, Margolis DM, Archin NM. 2014. Quantitation of replication-competent HIV-1 in populations of resting CD4+ T cells. J Virol 88:14070–14077. https://doi.org/10.1128/JVI.01900-14.
35. Brenchley JM, Hill BJ, Ambrozak DR, Price DA, Guenaga FJ, Casazza JP, Kuruppu J, Yazdani J, Migueles SA, Connors M, Roederer M, Douek DC, Koup RA. 2004. T-cell subsets that harbor human immunodeficiency virus (HIV) in vivo: implications for HIV pathogenesis. J Virol 78:1160–1168. https://doi.org/10.1128/JVI.78.3.1160-1168.2004.
36. Delobel P, Nugeyre MT, Cazabat M, Sandres-Saune K, Pasquier C, Cuzin L, Marchou B, Massip P, Cheynier R, Barre-Sinoussi F, Izopet J, Israel N. 2006. Naive T-cell depletion related to infection by X4 human immunodeficiency virus type 1 in poor immunological responders to highly active antiretroviral therapy. J Virol 80:10229–10236. https://doi.org/10.1128/JVI.00965-06.
37. Ostrowski MA, Chun TW, Justement SJ, Motola I, Spinelli MA, Adelsberger J, Ehler LA, Mizell SB, Hallahan CW, Fauci AS. 1999. Both memory and CD45RA+/CD62L+ naive CD4(+) T cells are infected in human immunodeficiency virus type 1-infected individuals. J Virol 73:6430–6435.
38. Wightman F, Solomon A, Khoury G, Green JA, Gray L, Gorry PR, Ho YS, Saksena NK, Hoy J, Crowe SM, Cameron PU, Lewin SR. 2010. Both CD31(+) and CD31(−) naive CD4(+) T cells are persistent HIV type 1-infected reservoirs in individuals receiving antiretroviral therapy. J Infect Dis 202:1738–1748. https://doi.org/10.1086/656721.
39. Bleul CC, Wu L, Hoxie JA, Springer TA, Mackay CR. 1997. The HIV coreceptors CXCR4 and CCR5 are differentially expressed and regulated on human T lymphocytes. Proc Natl Acad Sci U S A 94:1925–1930. https://doi.org/10.1073/pnas.94.5.1925.
40. Chahroudi A, Cartwright E, Lee ST, Mavigner M, Carnathan DG, Lawson B, Carnathan PM, Hashempoor T, Murphy MK, Meeker T, Ehnert S, Souder C, Else JG, Cohen J, Collman RG, Vanderford TH, Permar SR, Derdeyn CA, Villinger F, Silvestri G. 2014. Target cell availability, rather than breast milk factors, dictates mother-to-infant transmission of SIV in sooty mangabeys and rhesus macaques. PLoS Pathog 10:e1003958. https://doi.org/10.1371/journal.ppat.1003958.
41. Elliott ST, Wetzel KS, Francella N, Bryan S, Romero DC, Riddick NE, Shaheen F, Vanderford T, Derdeyn CA, Silvestri G, Paiardini M, Collman RG. 2015. Dualtropic CXCR6/CCR5 simian immunodeficiency virus (SIV) infection of sooty mangabey primary lymphocytes: distinct coreceptor use in natural versus pathogenic hosts of SIV. J Virol 89:9252–9261. https://doi.org/10.1128/JVI.01236-15.
42. Wetzel KS, Yi Y, Yadav A, Bauer AM, Bello EA, Romero DC, Bibollet-Ruche F, Hahn BH, Paiardini M, Silvestri G, Peeters M, Collman RG. 2018. Loss of CXCR6 coreceptor usage characterizes pathogenic lentiviruses. PLoS Pathog 14:e1007003. https://doi.org/10.1371/journal.ppat.1007003.
43. Eckstein DA, Penn ML, Korin YD, Scripture-Adams DD, Zack JA, Kreisberg JF, Roederer M, Sherman MP, Chin PS, Goldsmith MA. 2001. HIV-1 actively replicates in naive CD4(+) T cells residing within human lymphoid tissues. Immunity 15:671–682. https://doi.org/10.1016/S1074-7613(01)00217-5.
44. Kinter A, Moorthy A, Jackson R, Fauci AS. 2003. Productive HIV infection of resting CD4+ T cells: role of lymphoid tissue microenvironment and effect of immunomodulating agents. AIDS Res Hum Retroviruses 19:847–856. https://doi.org/10.1089/088922203322493012.
45. Avalos CR, Abreu CM, Queen SE, Li M, Price S, Shirk EN, Engle EL, Forsyth E, Bullock BT, Mac Gabhann F, Wietgrefe SW, Haase AT, Zink MC, Mankowski JL, Clements JE, Gama L. 2017. Brain macrophages in simian immunodeficiency virus-infected, antiretroviral-suppressed macaques: a functional latent reservoir. mBio 8:e01186-17. https://doi.org/10.1128/mBio.01186-17.
46. Estes JD, Kityo C, Ssali F, Swainson L, Makamdop KN, Del Prete GQ, Deeks SG, Luciw PA, Chipman JG, Beilman GJ, Hoskuldsson T, Khoruts A, Anderson J, Deleage C, Jasurda J, Schmidt TE, Hafertepe M, Callisto SP, Pearson H, Reimann T, Schuster J, Schoephoerster J, Southern P, Perkey K, Shang L, Wietgrefe SW, Fletcher CV, Lifson JD, Douek DC, McCune JM, Haase AT, Schacker TW. 2017. Defining total-body AIDS-virus burden with implications for curative strategies. Nat Med 23:1271–1276. https://doi.org/10.1038/nm.4411.
47. Hellmuth J, Valcour V, Spudich S. 2015. CNS reservoirs for HIV: implications for eradication. J Virus Erad 1:67–71.
48. McGary CS, Deleage C, Harper J, Micci L, Ribeiro SP, Paganini S, Kuri-Cervantes L, Benne C, Ryan ES, Balderas R, Jean S, Easley K, Marconi V, Silvestri G, Estes JD, Sekaly RP, Paiardini M. 2017. CTLA-4(+)PD-1(−) memory CD4(+) T cells critically contribute to viral persistence in antiretroviral therapy-suppressed, SIV-infected rhesus macaques. Immunity 47:776–788. https://doi.org/10.1016/j.immuni.2017.09.018.
49. Bolton DL, Minang JT, Trivett MT, Song K, Tuscher JJ, Li Y, Piatak M, Jr, O'Connor D, Lifson JD, Roederer M, Ohlen C. 2010. Trafficking, persistence, and activation state of adoptively transferred allogeneic and autologous simian immunodeficiency virus-specific CD8(+) T cell clones during acute and chronic infection of rhesus macaques. J Immunol 184:303–314. https://doi.org/10.4049/jimmunol.0902413.
50. Hu Y, Smyth GK. 2009. ELDA: extreme limiting dilution analysis for comparing depleted and enriched populations in stem cell and other assays. J Immunol Methods 347:70–78. https://doi.org/10.1016/j.jim.2009.06.008.
51. Diggle PJ, Liang K-Y, Zeger SL. 1994. Analysis of longitudinal data, p 68–69. Oxford University Press, Oxford, United Kingdom.